New Perspectives on the X-ray Emission of HD 104237 and Other Nearby Herbig Ae/Be Stars from *XMM-Newton* and *Chandra*

Stephen L. Skinner

CASA, Univ. of Colorado, Boulder, CO 80309-0389

Manuel Güdel

Paul Scherrer Institut, Würenlingen and Villigen, CH-5235 Switzerland

Marc Audard

Columbia Astrophysics Laboratory, Columbia Univ., 550 W. 120th St., New York, NY 10027

and

Kester Smith

Max Planck Inst. für Radioastronomie, Auf dem Hügel 69, D-53121 Bonn, Germany

ABSTRACT

The origin of the X-ray emission from Herbig Ae/Be stars is not yet known. These intermediate mass pre-main sequence stars lie on radiative tracks and are not expected to emit X-rays via solar-like magnetic processes, nor are their winds powerful enough to produce X-rays by radiative wind shocks as in more massive O-type stars. The emission could originate in unseen low-mass companions, or it may be intrinsic to the Herbig stars themselves if they still have primordial magnetic fields or can sustain magnetic activity via a nonsolar dynamo.

We present new X-ray observations of the nearby Herbig Ae star HD 104237 (= DX Cha) with *XMM-Newton*, whose objective is to clarify the origin of the emission. Several X-ray emission lines are clearly visible in the CCD spectra, including the high-temperature Fe Kα complex. The emission can be accurately modeled as a multi-temperature thermal plasma with cool (kT < 1 keV) and hot (kT $\gtrsim$ 3 keV) components. The presence of a hot component is compelling evidence that the X-rays originate in magnetically confined plasma, either in the Herbig star itself or in the corona of an as yet unseen late-type companion. The X-ray temperatures and luminosity (log L$_X$ = 30.5 ergs s^{-1}) are within the range expected for a T Tauri companion, but high resolution *Chandra* and *HST* images

constrain the separation of a putative companion to $<1''$. We place these new results into broader context by comparing the X-ray and bolometric luminosities of a sample of nearby Herbig stars with those of T Tauri stars and classical main-sequence Be stars. We also test the predictions of a model that attributes the X-ray emission of Herbig stars to magnetic activity that is sustained by a shear-powered dynamo.

Subject headings: stars: Herbig Ae/Be — stars: individual (HD 104237, HD 150193, HD 163296, R CrA, T CrA) — stars: pre-main sequence — X-rays: stars

1.   Introduction

The nearest star-forming regions are dominated by populations of young low-mass pre-main-sequence (PMS) stars, or T Tauri stars. Hundreds of T Tauri stars have now been identified in the Taurus-Auriga, Chamaeleon, and Rho Ophiuchus molecular clouds at distances of $\lesssim 160$ pc. Their masses are less than ~ 2 $M_\odot$ and they are the progenitors of late-type main sequence stars such as the Sun. In contrast, more massive PMS stars are rare in nearby star-forming regions. These elusive objects evolve rapidly onto the main sequence and can remain optically obscured during much of their PMS phase. However, a few nearby optically-bright PMS stars of intermediate mass (~ 2 - 10 $M_\odot$) are known. They are generally categorized as Herbig Ae/Be stars (Herbig 1960; Herbig & Bell 1988), which are thought to be more massive analogs of classical T Tauri stars (CTTS). They are often located in or near molecular clouds in the vicinity of T Tauri stars and have properties similar to CTTS including Hα emission, infrared excesses indicative of circumstellar material (disks, envelopes, or both), and poorly-understood photometric and spectroscopic variability (Appenzeller 1994; Finkenzeller & Mundt 1984, hereafter FM84; Herbig 1994; Hillenbrand et al. 1992). In addition, mass outflows are often detected (FM84; Garrison & Anderson 1977; Garrison 1978; Skinner, Brown, & Stewart 1993).

One of the nearest known Herbig Ae stars is HD 104237 (= DX Cha), lying in the recently discovered ϵ Cha group at a *Hipparcos* distance of 116 pc (Perryman et al. 1997; van den Ancker, de Winter, & Tjin A Djie 1988, hereafter AWD98). This star has attracted considerable observational attention because of its proximity, optical brightness (V = 6.6 mag), and relatively low visual extinction $A_V < 1$ mag. Its properties are summarized in Table 1. It does not lie in a molecular cloud but molecular gas has been detected in its vicinity (Knee & Prusti 1996) and age estimates range from ~ 2 - 5 My (AWD98; Feigelson, Lawson, & Garmire 2003, hereafter FLG03; Grady et al. 2004, hereafter G04). A spectral type of A4IVe was assigned in the early study of Hu et al. (1991), but more recent observations

with the *Hubble Space Telescope (HST)* suggest a later spectral type of A7IVe (Brown et al. 1997) or A7.5Ve - A8Ve (G04).

Observations with the *Infrared Space Observatory (ISO)* reveal a clear IR excess and a strong 10 μm silicate feature (Meeus et al. 2001). The IR excess can be modeled in terms of a passive irradiated disk with a small but uncertain outer radius of ∼10 - 20 AU (Dominik et al. 2003). The *HST* has traced a bipolar jet-like outflow (HH 669) with at least three emission knots down to angular separations of ≈0.125″ from the star (Woodgate et al. 2002; G04). There has also been a report of the detection of a close companion in *HST* and infrared images at a separation of 1.365″ ± 0.019″, possibly a M3-4 T Tauri star (Danks et al. 2001; G04).

ASCA detected HD 104237 as a moderately bright X-ray source, as reported by Skinner & Yamauchi (1996; hereafter SY96). The X-ray detection of HD 104237 has recently been confirmed in two higher angular resolution *Chandra* observations that were obtained as part of a limited snaphsot survey of Herbig stars (FLG03). This snapshot survey also detected the Herbig stars HD 100546 (B9Vne), HD 141569 (B9.5Ve), and HD 150193 (A1Ve). These high angular resolution *Chandra* detections substantiate earlier reports of X-ray emission from Herbig stars, including eleven X-ray detections obtained with the *Einstein* observatory (Damiani et al. 1994) and a surprisingly high detection rate of nearly 50% in a sample of 30 Herbig Ae/Be stars observed by *ROSAT* (Zinnecker & Preibisch 1994, hereafter ZP94; Preibisch & Zinnecker 1996).

The apparent presence of X-ray emission from Herbig stars is difficult to explain in the context of current theories of stellar X-ray emission. Herbig Be stars and earlier Ae stars are on radiative tracks and are not expected to have the outer convection zones needed to sustain internally-generated magnetic fields. Consequently, X-ray emission from magnetically-trapped coronal plasma such as occurs in the Sun and other cool stars is not expected. However, some recent evolutionary models such as those of Siess, Dufour, & Forestini (2000) suggest that later Herbig Ae stars of spectral types A6e - A8e could have very thin convection zones (Giardino et al. 2004), thus raising the interesting possibility of incipient solar-like magnetic activity in later Ae stars (see also Sec. 7.3). Finally, it is very unlikely that the X-ray emission of Herbig Ae stars arises in radiative wind shocks, as may be the case for much more massive O-type stars. The instabilities that are thought to produce X-ray emitting shocks in the supersonic winds of O stars are not predicted to occur in the more benign winds of Ae stars, which typically have velocities $v_\infty \approx$ 200 - 600 km s^{-1} and ionized mass loss rates $\dot{M} \leq 10^{-7}$ M$_\odot$ yr^{-1} (FM84; Skinner, Brown, & Stewart 1993). Furthermore, X-ray temperatures of several keV have now been detected in Herbig Ae stars (including HD 104237), and such temperatures are inconsistent with the soft emission predicted by

radiative wind shock models (SY96).

A possible explanation of the X-ray emission from Herbig stars is that it arises from faint late-type companions. However, *Chandra's* arcsecond angular resolution is now placing tight upper limits on the separation of such putative X-ray companions from the Herbig star. As discussed in more detail below, *Chandra* observations of HD 104237 show that the X-ray peak is offset by $<1''$ from the stellar optical position, thus ruling out the faint star seen $1.365''$ away by *HST* as the X-ray source. Although *Chandra's* angular resolution is not sufficient to exclude the presence of a cool secondary at separations of $<1''$, the recent *HST* observations fail to find any evidence for a T Tauri companion at separations $0.05'' < r \leq 1.0''$ (G04). This still does not rule out an unseen companion at $r \leq 0.05''$, but it is worth keeping in mind that other factors could lead to intrinsic X-ray emission from Herbig stars themselves. Of potential importance is their extreme youth and rapid rotation. Their ages are usually less than a few million years (Strom et al. 1972; Hillenbrand et al. 1992) and typical rotational velocities are $v\sin i \approx 80$ - 150 km s^{-1} (Finkenzeller 1985; Böhm & Catala 1995). Interestingly, a much lower value $v\sin i = 12 \pm 2$ km s^{-1} has been measured for HD 104237 by Donati et al. (1997). *HST* observations indicate that this low $v\sin i$ is probably a result of the system being viewed nearly pole-on at an inclination angle $i = 18°^{+14}_{-11}$ (G04).

Because of their youth, primordial magnetic fields inherited from the parent molecular cloud may still be present, and a marginal detection of a magnetic field in HD 104237 has been reported by Donati et al. (1997). It has also been suggested that the shear energy in a young rapidly-rotating star might give rise to a nonsolar dynamo, allowing an internally-generated field to be sustained in the youngest Herbig stars that decays rapidly over a few million years (Tout & Pringle 1995; Vigneron et al. 1990). If magnetic fields are indeed present, they could lead to magnetic plasma confinement and X-ray emission.

We present here new X-ray observations of HD 104237 obtained with *XMM-Newton* that were motivated by the unanswered question of the origin of X-ray emission from Herbig stars. The new data provide higher signal-to-noise CCD spectra and X-ray light curves than were previously available. Based on the inferred plasma properties, we argue for a magnetic origin for the X-ray emission. We use previously published and archived X-ray data for a distance-limited sample of Herbig stars to make comparisons with lower mass T Tauri stars and classical Be stars. We show that if Herbig stars are the evolutionary precursors of classical Be stars then a substantial falloff in the X-ray luminosities of Herbig stars is expected after they reach the main sequence, and a possible link with the similar behavior predicted by shear-dynamo theory is noted.

2. Observations

2.1. XMM-Newton Observations

Table 2 summarizes the *XMM-Newton* observations. Further information on the X-ray telescope is given by Jansen et al. (2001). Our analysis is based on CCD images, spectra, and light curves from the European Photon Imaging Camera (EPIC). Data were acquired simultaneously with the EPIC-PN camera (Strüder et al. 2001) and two nearly identical EPIC-MOS cameras (MOS-1 and MOS-2; Turner et al. 2001). The PN and MOS cameras provide a ≈30′ diameter field-of-view and energy coverage from ≈0.2 - 15 keV, moderate energy resolution (E/ΔE ≈ 20 - 50), and ≈6″ FWHM angular resolution on-axis.

Data reduction followed standard procedures using the *XMM-Newton* Science Analysis System software (SAS vers. 5.4.1). Pipeline-processed events files generated using the most current calibration data were filtered with *evselect* to select good event patterns. Spectra and light curves were extracted from the filtered events lists within a circular region of radius R_e ≈ 18″ centered on HD 104237 (Fig. 1). This radius corresponds to ≈75% of the encircled energy at 1.5 keV. Response matrix files (RMFs) and auxiliary response files (ARFs) tailored to the specific observational parameters were generated using the SAS tasks *rmfgen* and *arfgen*. The ARF file corrects the measured source flux for energy that falls outside of the R_e ≈ 18″ extraction region.

As discussed below (Sec. 3.0.1), four faint X-ray sources lie at separations of 4.1″ - 15″ from HD 104237. We attempted to remove some of the contamination these nearby sources by excluding events within small circular regions centered on their positions, which are accurately known from higher resolution *Chandra* images (Fig. 2). These smaller exclusion regions are shown as dashed circles in Figure 1. This strategy can remove some - but not all - of the contamination from these nearby sources. Specifically, sources B and C (Fig. 2) lie in the wings of the *XMM-Newton* point-spread function (PSF) at separations of 4.1″ - 5.8″ from HD 104237, and cannot be spatially resolved from the Herbig star at *XMM-Newton's* spatial resolution.

Background was extracted from source-free regions on the detector near HD 104237. Spectra were analyzed using XSPEC v. 11.1 and light curve analysis was undertaken with XRONOS v. 5.18 [1]. Spectra were rebinned to a minimum of 15 counts per bin for analysis

---

[1]Further information on XSPEC and XRONOS can be found at http://heasarc.gsfc.nasa.gov/lheasoft/xanadu. They are part of the XANADU software package maintained by the High Energy Astrophysics Science Archive Research Center (HEASARC) at NASA's Goddard Space Flight Center.

and all spectral models included an absorption component based on Morrison & McCammon (1983) cross sections.

2.2. Chandra Archive Observations of HD 104237

We have made use of two short ≈3 ks exposures of HD 104237 available in the *Chandra* public archive. Each of these exposures provides only ≈400 counts for HD 104237 and they are thus of limited use for spectral analysis. However, the images obtained with *Chandra's* higher angular resolution (90% encircled energy radius ≈2″ at 1.5 keV) and well-calibrated boresight provide crucial information on the position of the bright X-ray source relative to the optical position of HD 104237 as well as precise locations of fainter sources within ≈15″ of HD 104237. The positions of these fainter sources cannot be accurately measured in the lower resolution *XMM* images.

The *Chandra* observations were obtained with the ACIS-I detector in Faint/Timed mode on 5 June 2001 (ObsId 2404, 2.96 ks) and 4 Feb 2002 (ObsId 3428, 2.83 ks) with HD 104237 positioned ≈1.7′ off-axis. Level 2 data products generated during *Chandra X-ray Center* standard processing were further processed using CIAO software vers. 2.2.1 [2] in order to incorporate observation-specific bad pixel files and apply standard aspect corrections and energy filters. A more complete description of the *Chandra* observations can be found in FLG03, and *Chandra* instrumentation is described in the *Chandra Proposer's Observatory Guide (POG)* [3] and in Weisskopf et al. (2002).

3. Results

3.0.1. X-ray Images and Source Identification

Figure 1 shows the unsmoothed full resolution *XMM-Newton* image in the immediate vicinity of HD 104237 using summed data from the nearly identical MOS1 and MOS2 detectors. The MOS data provide somewhat better image quality than does PN because of the smaller 1.1″ MOS pixel size, which fully samples the telescope PSF. Figure 2 shows the same region imaged by *Chandra* ACIS-I on 4 Feb 2002. Both images clearly show a

---

[2]Further information on *Chandra Interactive Analysis of Observations (CIAO)* software can be found at http://asc.harvard.edu/ciao

[3]http://asc.harvard.edu/proposer/POG/

prominent X-ray source near the HD 104237 optical position, and the *Chandra* image also reveals four fainter sources within 15″ of HD 104237. These are labeled as B,C,D, and E for consistency with the notation used in FLG03. Additional information on the optical and X-ray properties of these four faint sources is given in FLG03 and G04.

The first *Chandra* image obtained on 5 June 2001 is similar to the second image shown in Figure 2 except that source C was not detected in the first observation. After applying the standard aspect correction to the first *Chandra* image and correcting the *Hipparcos* position for proper motion to the epoch of the *Chandra* observation, the position of the pixel having maximum brightness is offset by only 0.52″ from the *Hipparcos* position of HD 104237 (Perryman et al. 1997), and by 0.56″ from its near-IR position in the 2MASS Point Source Catalog. Similarly, the offsets between the *Chandra* peak positions of sources D and E and their 2MASS counterparts identified below are 0.54″ and 0.55″, respectively. Our comparison of the *Chandra* and 2MASS images suggests that these offsets could very likely be reduced to ≈0.2″ - 0.3″ by cross-registration. However, an astrometric solution was not attempted because of the small number of X-ray sources detected in the short *Chandra* exposures. Even without cross-registration, the above comparisons indicate that the *Chandra* positional accuracy relative to the *Hipparcos* and 2MASS frames is already better than 0.6″, in agreement with results from *Chandra* calibration studies [4].

Sources B and C are separated from HD 104237 by only 4.1″ - 5.8″ and cannot be clearly resolved at *XMM's* lower spatial resolution. Thus, our X-ray flux measurements based on *XMM-Newton* spectra will contain a small contribution from these two sources. Even so, their contribution to the total flux is expected to be minor since their respective *Chandra* count rates were ≤2% and ≈7% of the HD 104237 count rates. Sources D and E are offset from HD 104237 by ≈11″ - 15″ and are visible in the *XMM-Newton* image as extended structure to the southeast (Fig. 1). They were classified as T Tauri stars by FLG03 and are visible in the near-IR as 2MASS 12000829−7811395 and 2MASS 12000931−7811424. A comparison of the two *Chandra* observations shows that sources C and E are variable, but C is very faint (6 counts) and was only detected in the second observation.

Several other X-ray sources are present in the EPIC images, as listed in Table 3 and shown in Figure 3. The source list in Table 3 is based on a visual comparison of the PN and MOS images with the list of PN sources detected in the 0.5 - 4.5 keV range as part of the standard *XMM-Newton* pipeline processing. This processing uses the SAS sliding box detection algorithm *eboxdetect* along with maximum-likelihood task *emldetect* for PSF fitting. Table 3 includes only those PN sources that were also confirmed to be present in

---

[4]http://asc.harvard.edu/cal/ASPECT/

one or both MOS detectors, thus minimizing spurious detections at the risk of omitting some faint sources. Candidate near-IR or optical counterparts lying within 5″ of the X-ray positions were found for 9 of the 19 sources in Table 3, two of which are late-type stars. These identifications are based on searches of the 2MASS all-sky Point Source Catalog and the SIMBAD database.

The B9Vn star ϵ Cha lies $\approx$2.2′ southwest of HD 104237 and they form a common proper motion pair. Molecular gas has been detected around ϵ Cha and it may be a young object (Knee & Prusti 1996), but it lacks the emission lines needed to be classified as a Herbig Be star. We did not detect ϵ Cha with *XMM-Newton*, nor was it detected in the *Chandra* observations. The upper limit obtained from the EPIC PN image is log L_X (0.5 - 7 keV) $\leq$ 27.8 ergs s^{-1}. Here we have assumed a 1 keV thermal plasma spectrum with an absorption $N_H = 1.1 \times 10^{21}$ cm^{-2} corresponding to $A_V = 0.5$ mag (Knee & Prusti 1996), and a *Hipparcos* distance of 112 pc. The *Chandra* upper limit log $L_X \leq 27.7$ ergs s^{-1} (FLG03) is slightly more stringent because of *Chandra's* much lower detector background.

3.0.2. X-ray Variability

Figure 4 shows the background-subtracted EPIC-PN X-ray light curve of HD 104237 in the [0.5 - 5] keV range. We have used this restricted energy range for light curve analysis in order to minimize the possibility of contamination from soft and hard background photons.

No large-amplitude variations are visible in the PN light curve but a slow falloff in the count rate is apparent. This decline is also seen in the background-subtracted MOS light curves and in PN light curves constructed with other energy filters including a soft filter in the range [0.5 - 2.0] keV and a hard filter of [2.0 - 5.0] keV. The mean count rate for the PN light curve in Figure 4 is $\mu = 0.25 \pm 0.04$ c s^{-1} ($\pm 1\ \sigma$). During the first 4 ks of the observation the mean is $\mu = 0.27 \pm 0.03$ c s^{-1} while the last 4 ks gives $\mu = 0.23 \pm 0.03$ c s^{-1}. The probability of a constant count rate from a χ^2 analysis of the PN light curve binned at 200 s intervals is $P_{const} = 0.18$ and smaller values $P_{const} < 0.01$ are obtained from the summed MOS1 + MOS2 light curve.

As an additional check for variability, we have applied the Kolmogorov-Smirnov (KS) test (Press et al. 1992) to the unbinned PN event list, using events in the [0.5 - 5] keV range from a contiguous good-time interval during the last 9880 s of the observation. For the event extraction region shown in Figure 1, the KS test gives $P_{const} = 0.001$. If we instead use a simpler extraction region consisting of all events inside a small circle of radius $R_e = 8″$ centered on HD 104237, then the KS test gives $P_{const} = 0.068$.

The above results suggest that low-level variablity is quite likely present in the light curve. However, the origin of the variability remains ambiguous because of the nearby faint sources that are not clearly resolved from HD 104237 at *XMM-Newton's* angular resolution. Our analysis shows that the apparent low-level variability is present using source extraction regions centered on HD 104237 with radii as small as $R_e = 6'' - 7''$. Such a small extraction region excludes most of the photons from sources D and E, but contains photons from sources B and C in addition to those from HD 104237. Thus, sources D and E are not likely to be responsible for the variability. The most probable origin would then be HD 104237 itself, or sources B or C, or perhaps an as yet undetected close companion to HD 104237. We emphasize that even though the *XMM-Newton* observation has insufficient angular resolution to rule out variability from sources B or C, the two *Chandra* observations found no significant variability in source B and showed that source C is very faint (FLG03).

The two *Chandra* exposures were separated by eight months in time and provide an additional check for variability. Even though the exposures were short (≈ 3 ks each), there is little or no contamination of the X-ray light curves by nearby sources B,C,D, and E because of *Chandra's* higher angular resolution. The light curves show count rate fluctuations at the 2σ level but no statistically significant variability was found in either *Chandra* observation. However, the mean count rate during the second observation was somewhat higher than the first. The first observation detected 382 ± 20 counts in 2.96 ks within a circle of radius $3.9''$ centered on HD 104237, giving a mean rate in the 0.5 - 7 keV range $\mu = 0.13 \pm 0.01$ (1σ) c s^{-1}. Using the same extraction region, the second observation gave 477 ± 22 counts in 2.83 ks and $\mu = 0.17 \pm 0.01$ c s^{-1} (0.5 - 7 keV). These count rates may slightly underestimate the true values because of moderate photon pileup in ACIS-I. The $\approx 30\%$ higher count rate during the second observation may reflect real long-term variability, but the inferred change is of low statistical significance because of the scatter in the two light curves.

Slowly declining light curves similar to that detected by *XMM-Newton* have been seen in other pre-main sequence stars, such as the CTTS Haro 5-59 in Orion (Fig. 7 of Skinner, Gagné, & Belzer 2003). In some cases, the decline lasts for at least a day. The origin of such slow variability is not yet understood but possible explanations include the late decay phase of an X-ray flare that occurred prior to the observation or dynamical effects such as the rotation of an active region out of the line-of-sight. The absence of a detectable change in hardness ratio or temperature in the *XMM-Newton* light curve of HD 104237 suggests that the slow variability was due to a change in the emission measure, perhaps through dynamical effects. Obviously, longer term monitoring over timescales of days to weeks is needed to more accurately characterize the level of the variability and further constrain its origin.

3.0.3. XMM-Newton Spectra

Figure 5 shows the EPIC-PN spectrum, which provides a higher signal-to-noise (S/N) ratio for spectral analysis than the MOS. Three emission line features are clearly visible and are identified with transitions in the following He-like ions, where E_{lab} is the laboratory line energy and T_{max} (K) is the temperature at which the line emits maximum power: Si XIII (E_{lab} = 1.86 keV, log T_{max} = 7.0), Ca XIX (E_{lab} = 3.90 keV, log T_{max} = 7.4), and the Fe Kα complex which includes Fe XXV (E_{lab} = 6.67 keV, log T_{max} = 7.6). The individual components of the He-like triplets are not spectrally resolved by the PN or MOS detectors. The Fe Kα complex is confirmed in the lower S/N MOS spectra and provides unambiguous evidence for hot plasma.

Fluorescent Fe I Kα? In addition to the obvious line detections listed above, our analysis of the unbinned photon event list from the PN detector shows a weak feature at an energy slightly above 6.4 keV. A Gaussian fit of this feature gives a mean energy $\langle E \rangle$ = 6.46 [6.36 - 6.61; 90% conf.] keV. This feature is not present in the background spectrum. If real, this feature could be a weak detection of fluorescent emission from neutral iron (Fe I Kα) in cold material surrounding the star. Such fluorescent iron lines have recently been detected by *Chandra* in other hot stars such as the classical Be star γ Cas (Smith et al. 2004). However, we caution that: (i) the statistical significance of this detection is low, (ii) the feature is not seen in the lower S/N MOS data for HD 104237, and (iii) some blending of this feature with higher energy photons from the Fe Kα complex ($\approx$6.67 keV) could be present at the spectral resolution of the PN detector (which is $\approx$0.13 keV at 6.5 keV). It is thus clear that more sensitive observations will be needed to determine if Fe I Kα emission is indeed present.

X-ray Temperatures and EM Distribution: Acceptable fits of the spectrum were obtained using absorbed variable-abundance multi-temperature optically thin plasma models, as summarized in Table 4. For these fits, we used the *vapec* model as implemented in XSPEC v. 11.1. In addition, fits of comparable quality were obtained with the differential emission measure (DEM) model *c6pvmkl*, which approximates the DEM using a sixth order Chebyshev polynomial.

Single-temperature (1T) *vapec* models were not acceptable, but satisfactory fits were obtained using both two-temperature (2T) and three-temperature (3T) models, with 3T models giving slightly better fits as shown in Figure 5 (see also Table 4). The 2T and 3T models are qualitatively similar in that they both require cooler plasma at kT < 1 keV and a hotter component at kT $\approx$ 3 keV. However, the 3T model requires higher absorption and places a larger fraction of the total emission measure (EM) in cooler plasma below 1 keV. Acceptable fits were obtained with the 2T and 3T models using an Fe abundance that is consistent with solar, but an overabundance is inferred for Ca and perhaps Ne.

The hotter component at kT $\approx$ 3 keV is anticipated from high-temperature features such as the Fe Kα line complex and was also required to fit previous *ASCA* spectra (SY96). At lower temperatures, both the 2T and 3T models require a component at kT $\approx$ 0.6 keV and the 3T model yields a slight fit improvement to the low-energy part of the spectrum by adding a third very soft component at kT $\approx$ 0.15 keV whose EM is quite uncertain. This soft component is heavily absorbed and accounts for only $\approx$6% of the observed (absorbed) flux in the PN spectrum. Because of the marginal fit improvement gained by adding this very soft component, its low contribution to the observed flux, and calibration uncertainties at low energies, its physical reality is open to question. The acceptable fits obtained by both 2T and 3T models illustrate the ambiguity that is often present in physical interpretations of moderate resolution CCD spectra. The discrete-temperature 2T and 3T models are simple approximations of what is likely to be a more complex plasma temperature distribution.

DEM models also show a double-peaked structure with a cool peak below 1 keV and a hotter peak above 3 keV. The temperatures at which these peaks occur are somewhat sensitive to abundance assumptions but are typically in the range kT $\approx$ 0.25 - 0.6 keV for the cool component and kT $\approx$ 4 - 5 keV for the hot component. DEM models converge to an absorption $N_H \approx (1.9 - 2.0) \times 10^{21}$ cm^{-2}, which is consistent with the values derived from 3T models.

Abundances: Fits with the 2T *vapec* model using solar abundances (Anders & Grevesse 1989) were not acceptable. We thus allowed the abundances of Ne, Mg, Si, S, Ca, and Fe to vary, and in doing so were able to obtain acceptable fits (Table 4). The fit improvement obtained by using variable abundances is significant in the 2T model but marginal in the 3T model. Even though improved fits were obtained with variable abundances, it should be kept in mind that CCD spectra from PN and MOS provide only moderate spectral resolution and thus cannot provide definitive abundance estimates because of blended lines.

Only in the case of Ca did we find a significant departure from solar abundances, with values of 6.6 - 9.9 $\times$ solar inferred, albeit with large uncertainties (Table 4). This over-abundance is required to fit the line feature near 3.9 keV, which is identified as Ca XIX. Ar XVIII Lyβ also emits near this energy but we are unable to fit the feature by varying the Ar abundance. Also, there is no obvious detection of the Ar XVIII Lyα line near 3.3 keV, which should be several times stronger than the line near 3.9 keV in the temperature range of interest here. Thus, Ca XIX is the most likely line identification. Neon is the only other element whose abundance converges to nonsolar values at the 90% confidence level in *vapec* fits. The 2T and 3T *vapec* models yield a Ne abundance of about twice solar (Table 4).

Absorption and Visual Extinction: Using the results in Table 4 and the conversion from N_H to A_V of Gorenstein (1975), the 2T model implies a visual extinction $A_V = 0.35$ [0.24 - 0.48]

mag, while the 3T model gives $A_V = 1.01$ [0.54 - 1.40] mag, where brackets enclose 90% confidence intervals. DEM models give values $A_V \approx 0.9$ mag that are comparable to the 3T model. Optical studies based on the *Hipparcos* distance have given values in the range $A_V = 0.3$ mag (AWD98) to $A_V = 0.9$ mag (Malfait, Bogaert, & Waelkens 1998). Thus, the X-ray derived values are within the range inferred from optical data.

Extraction Region Comparisons: The above results are based on the extraction of source events using the region shown in Figure 1. In order to determine if the spectral analysis results are sensitive to the extraction region used, we extracted a PN spectrum using a simpler region consisting of all events inside a small circular region of radius $R_e = 8''$ centered on HD 104237. Fits of this spectrum with a 2T *vapec* model yielded nearly identical values of N_H, kT_1, and observed flux to those given in Table 4. The inferred value of kT_2 was $\approx 23\%$ less than that in Table 4, but its 90% confidence range overlaps that in Table 4. We thus conclude that our spectral analysis results are robust to changes in the source extraction region.

3.0.4. Chandra Spectra

We have analyzed the photon event lists for the two *Chandra* observations and extracted ACIS-I spectra as well as source-specific RMF and ARF files using the CIAO tool *psextract.* Because of the low number of counts (382 - 477 counts per spectrum), no corrections for charge transfer inefficiency were applied and we made use of *a priori* information on absorption and abundances from the *XMM-Newton* spectra to reduce the number of free parameters in spectral fits.

The photon energy distributions for HD 104237 are similar for the two *Chandra* observations. Using events in the 0.5 - 7 keV range, the mean photon energy in the first observation was $\langle E \rangle = 1.26 \pm 0.67$ (1σ) keV, while the second observation gave $\langle E \rangle = 1.40 \pm 0.83$ (1σ) keV.

We have fitted the spectrum of the second *Chandra* observation with a 2T *vapec* model, fixing the absorption N_H and abundances at the values determined from *vapec* model fits of the higher S/N *XMM-Newton* spectra (Table 4). The 2T *vapec* fit yields temperatures that are very similar to those obtained with *XMM*, namely $kT_1 = 0.76$ [0.64 - 0.84] keV and $kT_2 = 3.0$ [2.1 - 5.6] keV, where brackets enclose 90% confidence intervals. The observed (absorbed) flux of the second *Chandra* observation determined from the 2T *vapec* model is 22% less than that measured by *XMM-Newton* (Table 4). The 3T *vapec* model gives somewhat better agreement, with the observed *Chandra* flux being 10% less than that of

XMM-Newton (Table 4). Some (or perhaps all) of the excess flux measured by *XMM-Newton* relative to *Chandra* no doubt comes from the two faint nearby sources B and C, which cannot clearly be separated from HD 104237 at *XMM-Newton's* lower spatial resolution (Fig. 1).

4. X-ray Data for Other Nearby Herbig Stars

In the discussion below (Sec. 5), we will compare the properties of several nearby Herbig stars which have been detected in X-rays. Some of these detections are based on new or unpublished results, and we summarize these before proceeding.

Elias 1 (V892 Tau): This Herbig Ae star in the Taurus dark clouds was detected in the *ROSAT* survey of ZP94. A companion located $4.1''$ to the NE has been detected in high-resolution *VLA* radio observations (Skinner, Brown, & Stewart 1993) and in the near-infrared (Leinert et al. 1997). There is no definitive evidence so far of any companion at closer separations.

Giardino et al. (2004) have analyzed *Chandra* and *XMM-Newton* observations of Elias 1. Variability was detected in the $\sim$18 ks *Chandra* light curve, with impulsive changes in the count rate of a factor of two, suggestive of low-level flaring. Analysis of the *Chandra* spectrum with a 1T thermal plasma model gave a characteristic temperature kT $\approx$ 2 keV and log L_X (0.5 - 7.5 keV) = 30.2 ergs s^{-1}, the latter value being comparable to earlier *ROSAT* results (Table 5). The *XMM-Newton* observation detected a large high-temperature flare that was attributed to Elias 1, to within the *XMM-Newton* absolute pointing accuracy of $\approx 4''$.

The detection of rapid X-ray variability and hot plasma is a signature of magnetic activity. This is an important result if the emission is intrinsic to the Herbig star Elias 1 and not due to an as yet undetected lower mass companion. Because of the unusual X-ray properties of Elias 1, further searches for a close companion are clearly warranted.

HD 150193: This Herbig Ae star was detected as a double X-ray source in the 2.92 ks *Chandra* snapshot observation of FLG03, shown in Figure 6. A faint source (C) is located $\approx 1.36''$ NE (PA = $50° \pm 5°$) of the brighter X-ray peak (A). We use abbreviations (A) and (C) to identify bright X-ray peak and the faint source to its NE, consistent with the notation in FLG03. Near IR observations also show a double source, with the bright IR source being 2.2 mag brighter at K band and lying $1.1''$ NE (PA = $56°$) of the faint IR source (Pirzkal, Spillar, & Dyck 1997). The nearly identical separations and position angles suggest a one-to-one correspondence between the two sources seen in the X-ray and IR images. However, because of the close separation there is some ambiguity as to which source is the Herbig star.

Our measurements of the X-ray positions of the two sources in the aspect-corrected *Chandra* image (Fig. 6) indicate that the X-ray peak of the faint northerly source lies closer to the optical position of HD 150193, with a position offset of 0.6″. Thus, the faint X-ray source (C) is most likely the Herbig star. To match the relative geometry seen in the IR image, we then associate the faint northern X-ray source (C) with the bright northern IR source. That is, the Herbig star is faint in X-rays but bright in the near-IR. The X-ray bright source to the south is then associated with the fainter IR companion to the south. Note that this interpretation is different than that given by FLG03, who associated the brighter southern X-ray source (A) with the brighter northern IR source. In that case, there is no *Chandra* X-ray counterpart to the fainter southern IR source. We estimate 17 counts for the faint northern X-ray source (C) that we associate with HD 150193. The PIMMS simulator[5] then gives log L_X (0.5 - 7 keV) = 29.2 ergs s^{-1} (Table 5).

HD 163296: This Herbig star of spectral type A1Ve was observed for 10.7 ks with the *ROSAT* High Resolution Imager (HRI) on 31 March 1995. The archived image (rh202032n00) shows a clear detection of a source within 2″ of the optical position of HD 163296. Using PIMMS, the HRI count rate of 0.012 c s^{-1} gives an intrinsic luminosity log L_X (0.5 - 7 keV) = 29.8 ergs s^{-1} (Table 5). This value of L_X is very similar to that of other Herbig A0-1e stars such as AB Aur.

Close scrutiny of the apparent X-ray detection of HD 163296 is warranted because this star emits strongly in the UV (log T_{eff} (K) = 3.97, AWD98) and the HRI is known to be sensitive to UV radiation. This UV sensitivity was apparent in HRI calibration observations of the A0V star Vega (V = 0.03 mag), which gave a count rate of 0.10 c s^{-1} and a soft photon pulse height channel distribution. This count rate was much larger than expected based on HRI UV leak predictions (David et al. 1999; see also Berghöfer, Schmitt, & Hünsch 1999 and Barbera et al. 2000). A previous analysis concluded that the HRI count rate of HD 163296 was compatible with that expected for UV leaks (Grady et al. 2000). However, we have reexamined the HRI data and reach a different conclusion, as discussed below.

If we make the worst-case assumption that the Vega count rate was due entirely to UV leaks, then a calculation based on the V magnitude of HD 163296 (V = 6.85; Thé et al. 1985) gives a predicted count rate due to UV contamination of ≈1.9 × 10^{-4} c s^{-1}, which is ∼60 times less than observed. An alternative calculation using the HRI UV leak calibration derived by Berghöfer, Schmitt, & Hünsch (1999) and U = 6.99 mag for HD 163296 gives a predicted rate due to UV leaks of ≈1.3 × 10^{-5} c s^{-1}, or a factor of ∼900 less than observed.

---

[5]The Portable Interactive Multi-Mission Simulator (PIMMS) is a software tool developed and maintained by HEASARC at NASA's GSFC. For documentation, see http://heasarc.gsfc.nasa.gov/docs/software/tools.

In addition, we find that the pulse height channel distribution of photons detected from HD 163296 by HRI is significantly harder than that of Vega. Based on these UV leak count rate predictions and photon hardness considerations, we conclude that the HRI observation yielded a valid X-ray detection of HD 163296. We thus include HD 163296 in our analysis of Herbig star X-ray sources below.

R CrA and T CrA: These two stars are of interest because of their proximity in the nearby Corona Australis dark cloud. We assume a distance of 150 pc (FM84), but values in the literature range from 130 pc (Hillenbrand et al. 1992) to 170 pc (Knude & Høg 1998). R CrA has a variable spectrum (A1e - F7e) and T CrA is classified as F0-5e (FM84; Hillenbrand et al. 1992). Because of its later Fe spectral type, T CrA is not strictly a member of the Herbig star class but is often included in Herbig star catalogs because of its similar properties. Neither of these two stars was detected in the *ROSAT* survey of ZP94. We have analyzed an archived 19.7 ks *Chandra* observation of the CrA dark cloud obtained on 7 October 2000 (ObsId = 19) which shows a clear detection of R CrA and a probable detection of T CrA (Fig. 7). We obtain 68 ± 8 counts for R CrA and 4 ± 2 counts for T CrA in the 0.5 - 7 keV range. The emission from T CrA is faint but very likely real because of the low ACIS-I background (<1 count) and the good agreement between the stellar and X-ray positions (offset $= 0.97''$ after applying the recommended aspect correction). Using the PIMMS simulator, we obtain intrinsic luminosities $\log L_X$ (0.5 - 7 keV) = 29.1 for R CrA and $\log L_X = 27.9$ (ergs s^{-1}) for T CrA (Table 5). Since T CrA is a marginal detection, its L_X could be interpreted more conservatively as an upper limit.

5. X-ray Versus Bolometric Luminosities in Nearby Herbig Stars

Sensitive X-ray observations of several different star-forming regions have revealed a statistically significant correlation between the X-ray and bolometric luminosities of T Tauri stars. This correlation has been confirmed in *Chandra* observations of the young cluster IC 348 (Preibisch & Zinnecker 2002), the Orion Nebula Cluster (Feigelson et al. 2003), and the embedded infrared cluster in NGC 2024 (Skinner, Gagné, and Belzer 2003). These studies consistently find a ratio $\log (L_X/L_{bol}) \approx -3.75 \pm 1.0$, where the large scatter is probably due in part to X-ray flaring. A correlation of L_X with stellar mass was also found in IC 348 and the Orion Nebula Cluster. The physical origin of these correlations is not yet known but they are thought to be fundamentally linked to the X-ray emission process.

It would thus be of considerable interest to determine if a relation between L_X and L_{bol} also exists in Herbig stars, since they are thought to be more massive counterparts of CTTS. However, the observational issues are more complex in the case of Herbig stars. Unlike T

Tauri stars, there are no large codistant samples of Herbig stars in nearby clusters on which to base a statistical study. Instead, Herbig stars are sparsely distributed over many different star-forming regions spanning a range of uncertain distances and ages.

To make an initial comparison between L_X and L_{bol}, we have identified ten nearby Herbig stars (d $\lesssim$ 200 pc) whose distances are relatively well-known from *Hipparcos* parallaxes or by association with dark clouds. Their L_X and L_{bol} values are listed in Table 5 and plotted in Figure 8, normalized to the quoted distances. All stars in this subsample have been detected in X-rays and their L_X values were determined from recent *Chandra* observations (FLG03), the *ROSAT* survey of ZP94, and our own analysis of archived *Chandra* and *ROSAT* data. Bolometric luminosities were taken from the literature (AWD98; Berrilli et al. 1992). We note that there are conflicting values of the luminosity of Elias 1 in the literature (Berrilli et al. 1992; Hillenbrand et al. 1992). This subsample consists of stars of spectral type B9e or later and does not include early B-type stars, which typically lie beyond $\sim$500 pc and have very uncertain distances.

Since the data are based on an incomplete distance-limited sample, they do not answer the question of whether L_X and L_{bol} are correlated in the larger population of Herbig stars, of which more than 100 are presently known. However, several interesting trends can be seen in Figure 8. First, the values $-6.2 \leq \log (L_X/L_{bol}) \leq -4.7$ are clearly smaller than that observed for TTS and larger than that usually found in OB stars. This suggests that if the X-ray emission is intrinsic to the Herbig stars themselves (as opposed to a companion origin), then the efficiency of the X-ray emission process as gauged by L_X/L_{bol} ratios is lower than in TTS. Second, the range in $\log L_X$ is consistent with that found for TTS. Third, even for the restricted range in L_{bol} of this subsample, the scatter in L_X is large (± 1.0 dex) but is still comparable to the scatter observed in TTS.

Figure 8 also includes two emission-line stars of later Fe spectral type for which *Chandra* data exist. These are the weakly-detected star T CrA (F0-5e) and the spectroscopic binary AK Sco (F5+F5IVe; FLG03), which consists of two nearly identical Fe stars of masses $M_* \approx$ 1.4 $M_\odot$ in a 13.6 day orbit (Alencar et al. 2003). Even though these stars are not members of the Herbig Ae/Be class, they may be slightly lower mass analogs. Despite the nearly identical spectral types and similar L_{bol} values for these two stars, there is a remarkable difference in their L_X, with the binary AK Sco being more than an order of magnitude brighter in X-rays. This comparison shows that the presence of a companion has by some means greatly increased the X-ray output of AK Sco. It is tempting to speculate that the much fainter X-ray emission of T CrA may be more representative of young single Fe-type stars. However, there are hints that even T CrA may be a binary. Even though no companion was detected in K-band speckle images (Ghez et al. 1997), the position spectra

of Takami, Bailey, & Chrysostomou (2003) suggest that a faint companion could be present at a separation $>0.14''$. Since this lower limit is larger than the limit imposed by the Ghez et al K-band speckle images, Takami et al. concluded that if a companion is present it must be fainter than K = 10.5 mag.

6. Comparison With Classical Be Stars

Classical Be stars are B-type stars on or near the main sequence that exhibit line emission above the photospheric spectrum, as recently reviewed by Porter and Rivinius (2003). The evolutionary status of classical Be stars is not well-understood. However, they are rapid rotators, as are Herbig Ae/Be stars. This has led to the suggestion that Herbig stars might be the evolutionary precursors of classical Be stars (Finkenzeller 1985; Palla 1991).

Figure 8 shows the approximate region in the (L_{bol}, L_X) plane occupied by classical main-sequence BVe stars, based on a search of the *ROSAT* all-sky survey (RASS) catalog of optically bright OB stars compiled by Berghöfer, Schmitt, & Cassinelli (1996). Most BVe stars detected in the RASS had $29.5 < \log L_X \leq 31.0$ ergs s^{-1}, and a few undetected stars had upper limits as low as $\log L_X \leq 28.5$ ergs s^{-1}.

As can be seen in Figure 8, the range of L_X values for classical BVe stars is very similar to that of our Herbig star sample, but the L_X/L_{bol} ratios are clearly smaller for BVe stars. For BVe stars detected in the RASS, typical values are $\log (L_X/L_{bol}) = -6.4 \pm 0.5$, whereas the Herbig star sample has $\log (L_X/L_{bol}) = -5.4^{+0.8}_{-1.2}$. This comparison indicates that if the X-ray emission is intrinsic to the Herbig stars and if they do eventually evolve into classical Be stars, then their L_X/L_{bol} ratios must decline by roughly an order of magnitude after reaching the main sequence. Since no significant increase in L_{bol} is expected as a Herbig star evolves onto the main sequence, the above evolutionary scenario would imply that L_X must drop sharply. A dramatic decrease in L_X during the early main sequence phase is predicted by the shear-induced dynamo model, as discussed in more detail below (Sec. 7.3).

7. X-ray Emission Mechanisms

7.1. General Constraints on Emission Mechanisms

An analysis of several different possible X-ray emission mechanisms for HD 104237 was given by SY96 based on *ASCA* spectra. They examined the feasibility of wind shock and

accretion shock models as well as models involving magnetic confinement (coronae; wind-fed magnetospheres). They argued that shock models and magnetically-confined wind models could not explain the hotter plasma seen in the *ASCA* spectrum and concluded that the X-rays most likely originate in a magnetically confined region such as a corona. However, *ASCA*'s moderate angular resolution could not distinguish between X-ray emission from HD 104237 and other sources within $\approx 30''$, as can now be done (Fig. 2).

The spectral properties derived from the new *XMM-Newton* data are very similar to those obtained with *ASCA* and strengthen the previous conclusions of SY96. In particular, the existence of hot plasma at or above kT $\approx$ 3 keV ($\sim$35 MK) is now substantiated by the detection of high-temperature features such as the Fe K shell complex in the EPIC spectra. These high temperatures are incompatible with the predicted values of kT < 1 keV from wind shock and accretion shock models, assuming a wind speed $v_\infty \sim 500$ km s^{-1} and free-fall speed $v_{ff} \sim 560$ km s^{-1} for a Herbig Ae star of $\sim$2 M$_\odot$ (SY96). Shock models can account for the hotter plasma only if the actual wind speeds or infall speeds exceed the above estimates by a factor of two or more.

On the other hand, plasma temperatures of kT $\approx$ 3 keV are quite typical of magnetically active stars, including T Tauri stars. This value is well above the hydrogen escape temperature T$_{esc} \approx$ 13 MK (assuming M$_* =$ 2.3 M$_\odot$, R$_* =$ 2.7 R$_\odot$; Table 1) and it is therefore likely that the emission arises in magnetically-confined plasma. This could occur either in the corona of an as yet undetected late-type companion or perhaps in the Herbig star itself, as discussed further below.

7.2. X-ray Emission from Late-Type Companions

The companion hypothesis attributes the X-ray emission to a fainter low-mass companion star, rather than the Herbig star itself. This avoids the need to postulate magnetic fields in an intermediate mass star that is presumed to be non-convective, thus circumventing the contradiction with models based on the solar paradigm which associate magnetic fields with convection. Assuming that the companions are coeval with the Herbig star primary, they would most likely be T Tauri stars or perhaps optically-obscured class I infrared sources in the case of the youngest Herbig stars.

As already noted, fainter sources have been found in the immediate vicinity of HD 104237. These include the weak X-ray sources B and C detected by *Chandra* (Fig. 2) and the report of a faint star at an offset of 1.365$''$ and PA $=$ 254.6$°$ $\pm$ 0.35$°$ detected in *HST STIS* images (G04). However, it is obvious from the *Chandra* image in Figure 2 that the

faint sources B and C are not the origin of the strong X-ray emission detected at or near the HD 104237 optical position since they are clearly visible as secondary peaks lying $\approx$4″ - 6″ to the west.

It is also unlikely that the faint star at a separation of 1.365″ detected by *HST* is the origin of the X-ray emission associated with HD 104237, for three reasons. First, an offset of 1.365″ between the X-ray and optical positions would have been discerned at the positional accuracy of the *Chandra* image, which is better than 0.6″ (Sec. 3.0.1). Second, the position angle of this faint star relative to HD 104237 is inconsistent with the PA of the X-ray peak relative to the HD 104237 optical position. The centroid and peak-pixel X-ray positions lie $\approx$0.4″ - 0.5″ to the north of the *Hipparcos* optical position (Fig. 2), while the faint M-type companion lies 1.365″ to the W/SW at PA = 254.59° Third, the X-ray luminosity log L_X = 30.5 $\pm$ 0.1 (ergs s^{-1}) of the bright source detected here is at least an order of magnitude larger than typically observed for M3-4 TTS (e.g. Preibisch & Zinnecker 2002).

Since the M-type star at 1.365″ separation is not the primary X-ray source, the X-ray emission must arise from HD 104237 itself or from an as yet undetected companion at a separation $r < 1.365″$. Our comparison of the X-ray and optical positions (Fig. 2) indicates that the dominant X-ray source lies within 0.6″ of the Herbig star optical position. *HST* results provide an additional constraint by excluding a T Tauri companion at separations $0.05″ < r < 1.0″$ (G04). Taken together, the X-ray and *HST* observations imply that if the X-ray emission is due to an as yet undetected T Tauri companion, it must lie very close to HD 104237 at a separation $r \leq 0.05″$.

As Figure 7 shows, the X-ray luminosities determined for nearby Herbig stars are within the range observed for T Tauri stars. Also, the scatter in log L_X for this subsample of Herbig stars is $\pm$1.0 dex, which is comparable to that of TTS. Thus, from the standpoint of X-ray luminosities alone, one cannot exclude close T Tauri companions as the origin of the X-ray emission from Herbig stars. Assuming that all of the X-ray emission attributed to HD 104237 arises in an as yet undetected T Tauri companion, then the canonical relation log (L_X/L_{bol}) ≈ -3.75 for TTS yields a bolometric luminosity log $L_{bol} \approx 34.25$, or $L_{bol} \approx 4$ - 5 $L_\odot$ for the putative companion. However, this value is highly uncertain because of the scatter in the L_X versus L_{bol} relation for TTS.

7.3. Intrinsic X-ray Emission from Herbig Stars

The alternative to the companion hypothesis is that some, or all, of the X-ray emission is due to the Herbig star itself. Assuming that magnetic confinement is necessary to explain

the observed high-temperature plasma, then the emission could very well arise in a corona. Another possibility is a magnetically-confined wind shock, as has been proposed to explain the X-ray emission of some magnetic Ap-Bp stars such as IQ Aur (Babel & Montmerle 1997). However, this model gives temperature predictions kT < 1 keV that are similar to non-magnetic shock models, assuming wind speeds $v_\infty \approx$ 400 - 600 km s^{-1} typical of Herbig Ae stars. Thus, this model cannot explain the high-temperature plasma at kT $\gtrsim$ 3 keV.

In late-type stars, an outer convection zone is thought to be necessary to support magnetic (e.g. coronal) activity via a solar-like dynamo. The region in the HR diagram where surface convection zones first appear is somewhat uncertain, as recently reviewed by Favata & Micela (2003). However, the *ROSAT* detection of intrinsic X-ray emission from Altair (A7IV-V) (Schmitt 1997) provides compelling evidence that surface convection is already present in some late A-type stars. The recent classification of HD 104237 as A7.5Ve - A8Ve based on *HST* observations (G04) thus raises the interesting possibility that some of its X-ray emission might be associated with surface convection. However, the evolutionary tracks of Siess et al. (2000) suggest that a surface convection zone in HD 104237 would be quite thin, amounting to ≈0.9% of the stellar radius (assuming T_{eff} = 7300 K, log [$L_*/L_\odot$] = 1.42). It is not obvious why such a thin convection zone would give rise to an X-ray luminosity that is ~1000 times greater than that of Altair, which has a similar A7V spectral type. It may thus be that other factors, perhaps associated with youth, lead to elevated X-ray emission levels of Herbig stars - as discussed below.

It has been suggested that coronal X-ray emission could be sustained in a young rapidly-rotating Herbig star via a magnetic field set up by non-solar dynamo action that is powered by rotational shear energy. This possibility was explored by Vigneron et al. (1990) in the theoretical framework of sheared stratified fluids. A later development of this model by Tout & Pringle (1995, hereafter TP95) provides a quantitative prediction of the X-ray luminosity versus age, $L_X(t)$, but makes no temperature predictions. In the TP95 formulation,

$$L_X(t) \;=\; L_{Xo} \left[1 + \frac{t}{t_0} \right]^{-3} \tag{1}$$

In the above, the initial X-ray luminosity L_{Xo} depends on the stellar mass M_*, radius R_*, change in the star's angular velocity between its center and surface ($\Delta\Omega_0$), breakup velocity (Ω_k), and two dimensionless parameters of the theory ϵ and γ according to (eq. 4.4 of TP95)

$$\frac{L_{Xo}}{L_\odot} \;\sim\; 2.63 \times 10^{-3} \left[\frac{\epsilon}{10^{-3}} \right] \left[\frac{\gamma}{3 \times 10^{-5}} \right]^3 \left[\frac{\Delta\Omega_0}{\Omega_k} \right]^3 \left[\frac{M_*}{M_\odot} \right]^{2.5} \left[\frac{R_*}{R_\odot} \right]^{-2.5}. \tag{2}$$

For computational purposes, it is assumed that $\Delta\Omega_0/\Omega_k \sim 1$ (TP95). The parameters ϵ and γ are not well-determined empirically, with ϵ being the fraction of magnetic flux that is

dissipated at the stellar surface to heat coronal plasma and γ the efficiency of magnetic field generation. The decay timescale t_0 also depends on γ, M_*, and R_*. For fiducial values $\epsilon \sim 10^{-3}$ and $\gamma \sim 3 \times 10^{-5}$ (TP95), the decay timescale for Herbig Ae stars of mass $M_* \approx 2$ - 3 $M_\odot$ of interest here is $t_0 \sim 1$ - 2 My. Thus, this mechanism could sustain magnetic activity in a Herbig Ae star for a few million years, but drops off rapidly as t^{-3} thereafter.

A comparison of the predicted L_X from the above model with that measured for HD 104237 by *ASCA* was made by SY96. They assumed an earlier A4IVe spectral type, mass $M_* = 2.1$ $M_\odot$, radius $R_* = 2.6$ $R_\odot$, and age $t \sim 2$ My. For these parameters, the model underestimated the observationally-determined L_X by a factor of ~ 4. But the more recent *HST* data suggest a later A8Ve spectral type, $T_{eff} = 7300$ K, stellar luminosity $L_* = 26.3$ $L_\odot$, and an age $t \sim 5$ My (G04). Using these parameters, the evolutionary tracks of Siess et al. (2000) give $M_* = 2.14$ $M_\odot$ and $R_* = 3.0$ $R_\odot$. In that case, the decay timescale is $t_0 \sim 2.2$ My, and the model underestimates the X-ray luminosity (Table 1) by a factor of ~ 25. The above calculations show that uncertainties in ages, masses, and theoretical parameters such as ϵ and γ currently limit observational tests of the TP95 model to order-of-magnitude comparisons.

We have made additional comparisons of the predicted L_X from the TP95 model with the observed values listed for the other Herbig stars in Table 5. In these comparisons we have used stellar parameters given in the literature (i.e. AWD98) as well as our own estimates from the Siess et al. tracks, along with the fiducial values of ϵ and γ given above. Elias 1 was excluded from this comparison since it was not included in the AWD98 *Hipparcos*-based study and there are significant differences in reported values for its stellar luminosity and radius in the literature (e.g. Berrilli et al. 1992; Hillenbrand et al. 1992).

The model gives very good agreement for AB Aur and HD 97048, and it may be relevant that speckle techniques have so far failed to find any evidence for close companions around these two stars (Leinert, Richichi, & Haas 1997; Ghez et al. 1997). However, the model tends to underestimate L_X by as much as an order-of-magnitude in other cases, as already noted above for HD 104237. The discrepancy could be even larger for the B9Ve star HD 141569 if its age is $t > 10$ My (AWD98). However, a younger age $t \sim 5 \pm 3$ My has been inferred based on its association with two young M-type common proper motion companions (Weinberger et al. 2000). If this younger age is correct, then the model prediction is within an order of magnitude of the observed value for HD 141569.

8. Summary

The main results of this study are the following:

1. New X-ray spectra of the Herbig Ae star HD 104237 obtained with *XMM-Newton* provide the first clear detection of emission lines in this star, including Si XIII, Ca XIX, and the Fe Kα complex. The X-ray emission arises in an absorbed multi-temperature thermal plasma with cool (kT < 1 keV) and hot (kT $\gtrsim 3$ keV) components. The inferred X-ray absorption is equivalent to an extinction $A_V \approx 0.3$ - 1.0 mag, with best-fit models converging toward the high end of this range. This range is consistent with that determined from optical studies.

2. The presence of hot plasma at kT $\gtrsim 3$ keV is not consistent with shock model predictions, but is typical of values observed in magnetically-active PMS stars such as T Tauri stars. We conclude that the emission arises in magnetically-confined plasma, substantiating earlier *ASCA* results. The *XMM-Newton* light curve shows signs of slow variability at the $\approx 15\%$ level on a timescale of $\sim$hours, and a comparison of two *Chandra* observations taken eight months apart also suggests that low-level variability may be present. More persistent time monitoring over longer timespans is needed to confirm the suspected variability and constrain the timescale(s). If short-term ($\sim$hours) variability is confirmed, it would lend further support to a magnetic interpretation for the X-ray emission. The precise nature and location of the magnetically-confined region is not yet known, but a corona around the Herbig star (or an as yet unseen close companion) is a likely possibility.

3. Archived *Chandra* images show that the X-ray emission peak is offset by $<0.6''$ from the stellar optical position, which equates to a projected separation <70 AU at d $= 116$ pc. This small offset places stringent limits on the angular separation of a putative late-type X-ray companion, leaving open the possibility that some (or all) of the X-ray emission arises in the Herbig star itself.

4. The X-ray luminosities of a sample of ten Herbig Ae/Be stars with reliable distances are in the range $\log L_X = 29.9 \pm 1.0$ (ergs s^{-1}), which overlaps the range observed for T Tauri stars. Thus, X-ray emission from unseen T Tauri companions is not ruled out on the basis of L_X considerations. For this distance-limited Herbig star sample, we obtain a mean ratio $\log (L_X/L_{bol}) = -5.4^{+0.8}_{-1.2}$, which is less than for T Tauri stars and greater than for classical BVe stars. If the hypothesis that Herbig stars evolve into classical BVe stars is true, then the L_X values of Herbig stars must decrease dramatically after reaching the main sequence, and such a decrease is predicted by shear dynamo models.

5. The shear dynamo model of Tout & Pringle (1995) provides an alternative to the companion hypothesis for explaining X-ray emission in Herbig stars. A comparison of the predictions of this model against known L_X values for a sample of nine Herbig stars shows very good agreement in two cases (AB Aur and HD 97048). However, the model tends to underestimate L_X in all other cases by as much as an order of magnitude. Several factors could account for this disagreement including uncertain ages and masses, poorly-known model parameters that characterize magnetic processes, and excess X-ray emission from unseen lower mass companions.

This study strongly suggests that the X-ray emission detected within $0.6''$ of the HD 104237 optical position is of magnetic origin. The question that remains is whether the emission is coming from the Herbig star itself, or from an as yet undetected companion. The existing *Chandra* images show that if the emission is due to a companion, then its separation is $r < 1''$ from HD 104237. Recent *HST* images (G04) place a tighter constraint of $r < 0.05''$ on the separation of a T Tauri companion. Such a close companion, if present, cannot be spatially resolved with existing X-ray telescopes. Even so, further progress on the companion issue may nevertheless be possible at X-ray wavelengths. For example, high-quality images and spectra comparable to those of HD 104237 could be obtained for a much larger sample of Herbig stars, selected from the more than one hundred known and candidate members of the class (Thé, de Winter, & Pérez 1994). A more extensive X-ray data base would provide more complete information on plasma properties (kT, EM distribution), the X-ray luminosity function, and positional offsets. This information could then be used in statistical comparisons to determine if the X-ray properties of T Tauri stars are significantly different from Herbig Ae/Be stars.

Table 1.   Stellar Properties of HD 104237

Parameter	Value	Notes[a]
RA (J2000)	$12^h\ 00^m\ 05.0846^s$	(1)
Decl. (J2000)	$-78°\ 11'\ 34.564''$	(1)
Sp. Type	A4IVe; A7IVe; A7.5Ve - A8Ve	(2),(3),(4),(5)
d (pc)	116^{+8}_{-7}	(1)
V (mag.)	6.6	(6)
A_V (mag)	0.3 - 0.9	(7),(8)
J, H, K (mag)	5.8, 5.2, 4.6	(9)
Mass ($M_\odot$)	2.3	(7),(10)
$\log L_*$ ($L_\odot$)	$1.55^{+0.06}_{-0.05}$	(7),(10)
$\log L_X$ (ergs s^{-1})	30.5 ± 0.1	(11)

[a]Refs. and Notes: (1) *Hipparcos* position from Perryman et al. (1997), corrected for proper motion to epoch J2000.0 (2) Hu et al. (1991) (3) Eggen (1995) (4) Brown et al. (1997) (5) Grady et al. (2004) (6) SIMBAD (7) van den Ancker et al. (1998) (8) Malfait et al. (1998) (9) 2MASS Point Source Catalog (10) The quoted mass and L_* are from van den Ancker et al. (1998). The recent *HST* study of Grady et al. (2004) obtained $\log L_*$ ($L_\odot$) = $1.42^{+0.04}_{-0.07}$ and $T_{eff} \approx 7300$ K, for which the evolutionary tracks of Siess et al. (2000) give $M_* = 2.1\ M_\odot$. (11) this work; quoted value is the unabsorbed X-ray luminosity (0.5 - 7 keV) obtained by averaging the values obtained from 2T and 3T VAPEC models (Table 4)

Table 2.   XMM-Newton Observations of HD 104237

Parameter	Value
Start (UT)	17 Feb 2002 15:50
Stop (UT)	17 Feb 2002 19:52
Usable Exposure (ks)	12.2 (PN), 14.4 (per MOS)
ObsId / Revolution	0059760101 / 402
EPIC Mode	Imaging - Full Window
Optical Filter	Thick

Table 3.   XMM-Newton Sources[a]

No.	Name	R.A. (J2000)	Decl. (J2000)	Net Counts	Identification
1	J115646.4−781325	11 56 46.47	-78 13 25.0	42 ± 12	...
2	J115908.7−781234	11 59 08.76	-78 12 34.6	72 ± 14	2M 11590798-7812322
3	J115913.6−782409	11 59 13.62	-78 24 09.7	54 ± 13	...
4	J115932.3−782223	11 59 32.37	-78 22 23.1	90 ± 14	...
5	J115943.4−775838	11 59 43.41	-77 58 38.4	66 ± 14	...
6*	J115948.0−781147	11 59 48.06	-78 11 47.4	46 ± 12	2M 11594807-7811450; CPD−77° 773
7*	J120005.9−781136	12 00 05.93	-78 11 36.6	7167 ± 81	2M 12000511-7811346; HD 104237
8*	J120048.3−781107	12 00 48.33	-78 11 07.6	47 ± 12	...
9*	J120049.6−781001	12 00 49.63	-78 10 01.9	57 ± 18	2M 12004942-7809574; CPD−77° 775
10	J120054.9−782030	12 00 54.92	-78 20 30.7	38 ± 11	2M 12005517-7820296
11	J120059.8−781658	12 00 59.85	-78 16 58.8	122 ± 32	...
12*	J120118.6−780254	12 01 18.60	-78 02 54.3	56 ± 17	2M 12011809-7802522
13*	J120119.9−775947	12 01 19.97	-77 59 47.5	217 ± 33	2M 12012042-7759478
14	J120135.7−780428	12 01 35.75	-78 04 28.9	89 ± 21	...
15	J120137.9−781832	12 01 37.95	-78 18 32.2	38 ± 11	2M 12013691-7818345
16	J120139.0−782120	12 01 39.04	-78 21 20.2	67 ± 20	...
17	J120153.2−781842	12 01 53.25	-78 18 42.2	94 ± 14	2M 12015251-7818413
18	J120156.5−780605	12 01 56.57	-78 06 05.3	38 ± 11	...
19*	J120235.0−781059	12 02 34.96	-78 10 59.3	92 ± 21	...

[a]Sources are included in this table if they were detected in PN and in one or both MOS. An asterisk in column (1) indicates that additional source notes follow below. Net counts are from EPIC-PN pipeline processing source list, and are background-subtracted and PSF-corrected in the 0.5 - 7.5 keV range. Candidate infrared and optical identifications are listed if they lie within $5''$ of the X-ray position. Infrared identifications are from the 2MASS (2M) all-sky Point Source Catalog, and optical identifications are from SIMBAD.

NOTES:

6. The K0 star CPD−77° 773 is offset by $2.4''$ from the X-ray position. Source lies near CCD gap; net counts may be underestimated.

7. Counts include nearby sources B,C,D, E (Fig. 2).

8. Not detected by pipeline processing, but visible in PN and MOS. Position is from MOS.

9. The multiple star CPD−77° 775 is offset by $4.7''$ from the X-ray position.

12. Visible in PN but only weakly detected in MOS2.

13. Possible double or extended X-ray source. Peak position is from MOS.

19. Source lies near CCD gap; net counts uncertain.

Table 4. *XMM-Newton* Spectral Fit Results for HD 104237

Parameter	2T VAPEC	3T VAPEC
N_H (10^{21} cm^{-2})	0.78 [0.53 - 1.06]	2.25 [1.20 - 3.10]
kT_1 (keV)	0.58 [0.38 - 0.62]	0.58 [0.46 - 0.63]
EM_1 (10^{52} cm^{-3})	4.46 [3.14 - 6.84]	6.71 [2.91 - 9.06]
kT_2 (keV)	3.18 [2.78 - 3.47]	2.92 [2.54 - 3.34]
EM_2 (10^{52} cm^{-3})	8.58 [7.34 - 10.1]	9.26 [7.02 - 10.5]
kT_3 (keV)	$\cdots$	0.15 [0.11 - 0.20]
EM_3 (10^{52} cm^{-3})	$\cdots$	8.95 [1.79 - 12.0]
Abundances	varied[a]	varied[b]
χ^2/dof	221.0/217	208.8/215
χ^2_{red}	1.02	0.96
F_X (10^{-12} ergs cm^{-2} s^{-1})	1.30 (1.53)	1.32 (2.41)
L_X (10^{30} ergs s^{-1})	2.46	3.88

Note. — Based on fits of the EPIC PN spectrum binned to a minimum of 15 photons per bin (Fig. 5) with the VAPEC optically thin plasma model. The tabulated parameters are absorption column density (N_H), plasma temperature (kT), and emission measure (EM). Brackets enclose 90% confidence intervals. X-ray flux (F_X) is the observed (absorbed) value followed in parentheses by the unabsorbed value in the 0.5 - 7.0 keV range. X-ray luminosity (L_X) is the unabsorbed value in the 0.5 - 7.0 keV range. The flux excludes counts in the proximity of faint nearby sources detected in higher spatial resolution *Chandra* observations (Figs. 1 and 2). A distance of 116 pc is assumed.

[a]Best-fit abundances relative to the solar values of Anders & Grevesse (1989) and 90% confidence intervals were: Ne = 2.3 [1.3 - 4.3], Mg = 2.0 [1.4 - 2.7], Si = 2.0 [1.2 - 3.2], S = 0.7 [0.0 - 2.3], Ca = 9.9 [4.5 - 14.7], Fe = 0.8 [0.5 - 1.1].

[b]Best-fit abundances relative to the solar values of Anders & Grevesse (1989) and 90% confidence intervals were: Ne = 2.2 [1.3 - 4.9], Mg = 1.7 [1.0 - 4.0], Si = 1.6 [1.0 - 3.7], S = 0.6 [0.0 - 2.1], Ca = 6.6 [1.5 - 13.1], Fe = 1.0 [0.7 - 1.8].

Table 5.   X-ray Detections of Nearby Herbig Ae/Be Stars and Fe Stars [a]

No.	Name	Sp. Type	d (pc)	log L_{bol} (ergs s^{-1})	log L_X (ergs s^{-1})	X-ray refs.
1*	HR 5999	A5-7III/IVe	210^{+50}_{-30}	35.51	30.78	(1)
2	HD 104237	A4IVe	116^{+8}_{-7}	35.13	30.50	(2,3,4)
3*	Elias 1	A0-6e	140^{+20}_{-20}	35.16	30.28	(1,5)
4	HD 141569	B9.5Ve	99^{+9}_{-8}	34.93	30.10	(2)
5*	HD 163296	A1Ve	122^{+17}_{-13}	35.06	29.80	(6)
6*	AB Aur	A0Ve	144^{+23}_{-17}	35.26	29.50	(1)
7	HD 100546	B9Vne	103^{+7}_{-6}	35.09	29.40	(2)
8*	HD 150193	A1Ve	150^{+50}_{-30}	35.05	29.25	(7)
9*	R CrA	A1e-F7e (var)	150^{+30}_{-30}	35.74	29.09	(7)
10*	HD 97048	B9-A0e	180^{+30}_{-20}	35.19	28.96	(1)
11*	AK Sco	F5+F5IVe	150^{+40}_{-30}	34.46	29.10	(2)
12*	T CrA	F0-5e	150^{+30}_{-30}	34.58	27.88	(7)

[a]Hipparcos distances, spectral types, and L_{bol} are from AWD98, except as follows. Distance of Elias 1 (= V892 Tau) is from Elias (1978), and distances of R and T CrA are from FM84. The L_{bol} values of Elias 1, R and T CrA are from Berrilli et al. (1992). All luminosities have been adjusted to the quoted distances and L_X values are unabsorbed. X-ray refs.: (1) ZP94 (*ROSAT*), (2) FLG03 (*Chandra*), (3) this work (*XMM*), (4) SY96 (*ASCA*), (5) Giardino et al. 2004 (*Chandra*), (6) this work (*ROSAT* HRI archive), (7) this work (*Chandra* archive).

Note. —

1. L_X is from ZP94, adjusted to 210 pc.

3. Spectral type has been listed as A0 (FM84) or A6e (HB88).

5. L_X is from PIMMS, using *ROSAT* HRI rate 0.012 c s^{-1}, $N_H = 5.5 \times 10^{20}$ cm^{-2} ($A_V = 0.25$ mag), and 1 keV Raymond-Smith (RS) plasma model. See text.

6. L_X is from PIMMS, using *ROSAT* PSPC rate 8.85×10^{-3} c s^{-1} (ZP94), $N_H = 1.1 \times 10^{21}$ cm^{-2} ($A_V = 0.5$ mag), and 1 keV RS plasma model.

8. L_X is from PIMMS, using *Chandra* ACIS-I rate 5.82×10^{-3} c s^{-1}, $N_H = 3.5 \times 10^{21}$ cm^{-2} ($A_V = 1.6$ mag), and 1 keV RS plasma model. See text.

9. L_X is from PIMMS, using *Chandra* ACIS-I rate 3.45×10^{-3} c s^{-1}, $N_H = 4.4 \times 10^{21}$ cm^{-2} ($A_V = 2$ mag), and 1 keV RS plasma model. See text.

10. L_X is from PIMMS, using *ROSAT* PSPC rate 1.14×10^{-3} c s^{-1} (ZP94), $N_H = 2.7 \times 10^{21}$ cm^{-2} ($A_V = 1.2$ mag), and 1 keV RS plasma model.

11. SB2 with 13.6 d orbital period (Alencar et al. 2003).

12. L_X is from PIMMS, using *Chandra* ACIS-I rate 2.02×10^{-4} c s^{-1}, $N_H = (3.8$

- 4.7) $\times 10^{21}$ cm^{-2} (A$_V$ = 1.7 - 2.1 mag), and 1 keV RS plasma model. See text.

REFERENCES

Alencar, S.H.P. et al. 2003, A&A, 409, 1037

Anders, E., & Grevesse, N. 1989, Geochim. Cosmochim. Acta, 53, 197 (AG89)

Appenzeller, I. 1994, in *The Nature and Evolutionary Status of Herbig Ae/Be Stars*, A.S.P. Conf. Series v. 62, ed. P.S. Thé, M.R. Pérez, and E.P.J. van den Heuvel (San Francisco: ASP), 12

Babel, J. & Montmerle, T. 1997, A&A, 323, 121

Barbera, M., Micela, G., Collura, A., Murray, S.S., & Zombeck, M.V. 2000, ApJ, 545, 449

Berghöfer, T.W., Schmitt, J.H.M.M., & Cassinelli, J.P. 1996, A&AS, 118, 481

Berghöfer, T.W., Schmitt, J.H.M.M., & Hünsch, M. 1999, A&A, 342, L17

Berrilli, F., Corciulo, G., Ingrosso, G., Lorenzetti, D., Nisini, B., & Strafella, F. 1992, ApJ, 398, 254

Böhm, T. & Catala, C. 1995, A&A, 301, 155

Brown, A., Tjin A Djie, H.R.E, Blondel, P.F.C., Harper, G.M., Bennett, P.D., & Skinner, S.L. 1997, in Accretion Phenomena and Related Outflows, IAU Colloq. 163, ASP Conf. Ser. v. 121, ed. D.T. Wickramasinghe, G.V. Bicknell, & L. Ferrario (San Francisco: ASP), 448

Danks, A. et al., 2001, BAAS (AAS Meeting 199), 33, Abstract 60.14

Damiani, F., Micela, G., Sciortino, S., & Harnden, F.R. 1994, ApJ, 436, 807

David, L.P. et al. 1999, The ROSAT High Resolution Imager (HRI) Calibration Report, http://hea-www.harvard.edu/rosat/

Dominik, C., Dullemond, C.P., Waters, L.B.F.M., & Walch, S. 2003, A&A, 398, 607

Eggen, O.J. 1995, AJ, 110, 1749

Elias, J.H. 1978, ApJ, 224, 857

Favata, F. & Micela, G. 2003, Sp. Sci. Rev., 108, 577

Feigelson, E.D., Gaffney, J.A., Garmire, G., Hillenbrand, L.A., & Townsley, L. 2003, ApJ, 584, 911

Feigelson, E.D., Lawson, W.A., & Garmire, G.P. 2003, ApJ, in press (FLG03)

Finkenzeller, U. 1985, A&A, 151, 340

Finkenzeller, U. & Mundt, R. 1984, A&AS, 55, 109 (FM84)

Garrison, L.M. 1978, ApJ, 224, 535

Garrison, L.M. & Anderson, C.M. 1977, ApJ, 218, 438

Giardino, G., Favata, F., Micela, G., & Reale, F. 2004, A&A, 413, 669

Ghez, A.M.,McCarthy, D.W., Patience, J.L., & Beck, T.L. 1997, ApJ, 481, 378

Gorenstein, P. 1975, ApJ, 198, 95

Grady, C.A. et al. 2000, ApJ, 544, 895

Grady, C.A. et al. 2004, ApJ, in press, ApJ preprint doi:10.1086/420763 (G04)

Herbig, G.H. 1960, ApJS, 4, 337

Herbig, G.H. 1994, in *The Nature and Evolutionary Status of Herbig Ae/Be Stars*, A.S.P.
    Conf. Series v. 62, ed. P.S. Thé, M.R. Pérez, and E.P.J. van den Heuvel (San Francisco:
    ASP), 3

Herbig, G.H. & Bell, K.R. 1988, Third Catalog of Emission-Line Stars of the Orion Popula-
    tion, Lick Observatory Bull. 1111, Univ. California, Santa Cruz (HB88)

Hillenbrand, L.A., Strom, S.E., Vrba, F.J., & Keene, J. 1992, ApJ, 397, 613

Hu, J.Y. et al. 1991, A&A, 248, 150

Jansen, F. et al., 2001, A&A, 365, L1

Knee, L.B.G. & Prusti, T. 1996, A&A, 312, 455

Knude, J. & Høg, E. 1998, A&A, 338, 897

Leinert, C., Richichi, A., & Haas, M. 1997, A&A, 318, 472

Malfait, K., Bogaert, E., & Waelkens, C. 1998, A&A, 331, 211

Meeus, G., Waters, L.B.F.M., Bouwman, J., van den Ancker, M.E., Waelkens, C., & Malfait,
    K. 2001, A&A, 365, 476

Morrison, R. & McCammon, D. 1983, ApJ, 270, 119

Palla, F. 1991, in Angular Momentum Evolution of Young Stars, ed. S. Catalano & J.R. Stauffer (Dordrecht: Kluwer), 21

Perryman, M.A.C. et al. 1997, A&A, 323, 49

Pirzkal, N., Spillar, E.J., & Dyck, H.M. 1997, ApJ, 481, 392

Porter, J.M. & Rivinius, T. 2003, PASP, 115, 1153

Preibisch, T. & Zinnecker, H. 1996, in *Röntgenstrahlung from the Universe*, ed. H. Zimmerman & J. Trümper (Garching: MPE), 17 (PZ96)

Preibisch, T. & Zinnecker, H. 2002, AJ, 123, 1613

Press, W.H., Teukolsky, S.A., Vetterling, W.T., & Flannery, B.P. 1992, Numerical Recipes in Fortran (New York: Cambridge U. Press), 617

Siess, L., Dufour, E., & Forestini, M. 2000, A&A, 358, 593

Schmitt, J.H.M.M. 1997, A&A, 318, 215

Skinner, S.L., Brown, A., & Stewart, R.T. 1993, ApJS, 87, 217

Skinner, S.L., Gagné, M., & Belzer, E. 2003, ApJ, 598, in press

Skinner, S.L. & Yamauchi, S. 1996, ApJ, 471, 987 (SY96)

Smith, M.A., Cohen, D.H., Gu, M.F., Robinson, R.D, Evans, N.R., & Schran, P.G. 2004, ApJ, 600, 972

Strom, S.E., Strom, K.M., Yost, J., Carrasco, L., & Grasdalen, G. 1972, ApJ, 173, 353

Takami, M., Bailey, J., & Chrysostomou, A. 2003, A&A, 397, 675

Thé, P.S., de Winter, D., & Pérez, M.R. 1994, A&AS, 104, 315

Thé, P.S., Felenbok, P., Cuypers, H., & Tjin A Djie, H.R.E. 1985, A&A, 149, 429

Tout, C.A. & Pringle, J.E. 1995, MNRAS, 272, 528 (TP95)

Turner, M.J.L. et al. 2001, A&A, 365, L27

van den Ancker, M.E., de Winter, D., & Tjin A Djie, H.R.E. 1998, A&A, 330, 145 (AWD98)

Vigneron, C., Mangeney, A., Catala, C., & Schatzman, E. 1990, Sol. Phys., 128, 287

Weinberger, A.J., Rich, R.M., Becklin, E.E., Zuckerman, B., & Matthews, K. 2000, ApJ, 544, 937

Weisskopf, M.C., Brinkman, B., Canizares, C., Garmire, G., Murray, S., & Van Speybroeck, L.P. 2002, PASP, 114, 1

Woodgate, B. et al., 2002, BAAS, 34(4), 1136

Zinnecker, H. & Preibisch, T., 1994, A&A, 292, 152 (ZP94)

Fig. 1.— Unsmoothed linearly-scaled *XMM-Newton* image of the region near HD 104237 obtained by combining photons from the MOS1 and MOS2 detectors in the 0.3 - 7 keV range. The pixel size is 1.1″ and the coordinate overlay is J2000. Spectra and light curves of HD 104237 were extracted using photons inside the solid circle of radius 18″ centered on the star, excluding those photons that fell inside the dashed circles surrounding the faint sources B,C,D, and E detected in higher-resolution *Chandra* images (Fig. 2). *Chandra* positions of the four faint sources are marked with crosses.

Fig. 2.— Unsmoothed aspect-corrected *Chandra* ACIS-I image of the region near HD 104237 obtained in a 2.86 ks observation on 4 Feb. 2002 with HD 104237 located 1.7′ off-axis. The pixel size is 0.49″ and the energy range is 0.3 - 7 keV, with a J2000 coordinate overlay and linear scaling. The asterisk at center marks the *Hipparcos* position of HD 104237 (Table 1). The *Hipparcos* position is offset by 0.52″ from the X-ray *peak* position, which is (J2000.) RA = $12^h\ 00^m\ 05.062^s$, decl. = $-78°\ 11'\ 34.06''$. The *Hipparcos* position is offset by 0.4″ from the X-ray *centroid* position, which is RA = $12^h\ 00^m\ 05.089^s$, decl. = $-78°\ 11'\ 34.16''$. Crosses mark the positions of four fainter X-ray sources B,C,D, and E whose properties are summarized in Tables 3 and 5 of FLG03.

Fig. 3.— Wavelet-smoothed *XMM-Newton* EPIC-PN image of the region surrounding HD 104237. The intensity scale is logarithmic and the energy range is 0.3 - 7 keV, with a J2000 coordinate overlay. The circled sources correspond to objects detected in PN and MOS, as listed in Table 3.

Fig. 4.— Background-subtracted *XMM-Newton* X-ray light curve of HD 104237 using photons from the EPIC PN detector in the 0.5 - 5 keV energy range and a bin size of 200 s (filled squares). The light curve was extracted using the region shown in Figure 1, which excludes some photons in the vicinity of faint sources B,C,D, and E. The background light curve at bottom was extracted from a source-free region on the same CCD as HD 104237 and is binned at 600 s intervals. The mean count rate and standard deviation for the source light curve (top) is 0.25 ± 0.04 c s^{-1} and the corresponding value for the background light curve (bottom) is 0.007 ± 0.004 s^{-1}. Error bars are 1σ.

Fig. 5.— Background-subtracted *XMM-Newton* X-ray spectrum of HD 104237 using photons from the EPIC PN detector and the extraction region shown in Figure 1. The spectrum has been rebinned to a minimum of 15 photons per energy bin. Solid line shows the best-fit 3T VAPEC optically thin plasma model (Table 4). The best-fit 2T VAPEC model (Table 4) is nearly identical to the 3T model shown, except that the 2T model slightly underestimates the flux in the 0.5 - 0.6 keV range by $\approx 20\%$.

Fig. 6.— Unsmoothed *Chandra* ACIS-I image of the Herbig Ae star HD 150193 in the 0.3 - 7 keV range with linear scaling and J2000 coordinates. The pixel size is 0.49″. The cross marks the optical position of HD 150193, and circled sources A and C correspond to the bright X-ray peak and a fainter X-ray peak to its NE. The X-ray position of the faint peak C is RA = $16h$ $40m$ $17.94s$, Decl. $= -23° 53' 44.64''$. which is offset by 0.6″ from the optical position, as compared to a 0.8″ offset for the bright peak A. The faint peak C is identified with the Herbig star HD 150193.

Fig. 7.— Unsmoothed archived *Chandra* ACIS-I image of the Corona Australis cloud (ObsId = 19) in the 0.3 - 7 keV range. The usable exposure is 19.7 ks and coordinate overlay is J2000. The circled detection of R CrA has 68 ± 8 counts and weak emission (4 ± 2 counts) is seen at the position of T CrA.

Fig. 8.— X-ray and bolometric luminosities of Herbig Ae/Be stars (filled squares), whose numbers correspond to Table 5. Also shown are the Fe stars AK Sco and T Cra (open squares). The stellar luminosity of Elias 1 is uncertain (Berrilli et al. 1992; Hillenbrand et al. 1992). The large solid polygon to the left encloses the region occupied by T Tauri stars and the sloping dashed line shows the typical relation log $(L_X/L_{bol}) = -3.75$ for TTS. The solid polygon on the right shows the analogous region for massive OB stars and their canonical relation log $(L_X/L_{bol}) = -7.0$. The dotted polygon at right center encloses the region occupied by classical main-sequence BVe stars. The Herbig stars shown are (1) HR 5999, (2) HD 104237, (3) Elias 1 (= V 892 Tau), (4) HD 141569, (5) HD 163296, (6) AB Aur, (7) HD 100546, (8) HD 150193, (9) R CrA, (10) HD 97048.
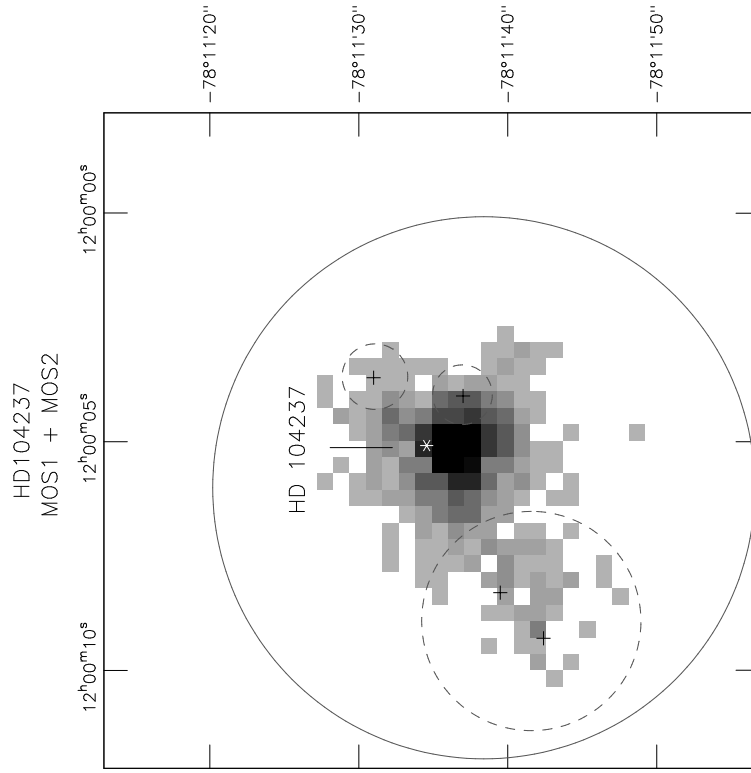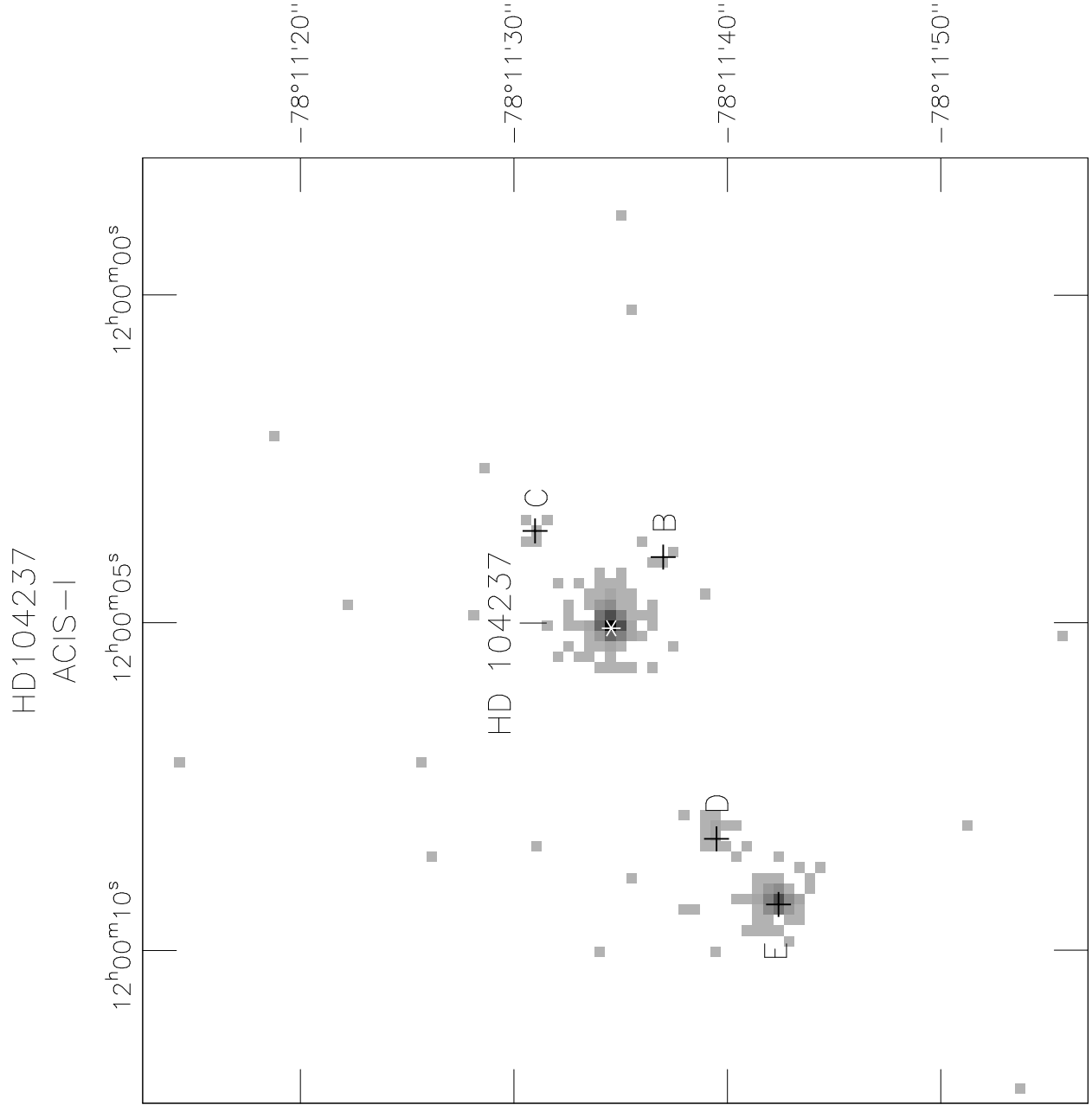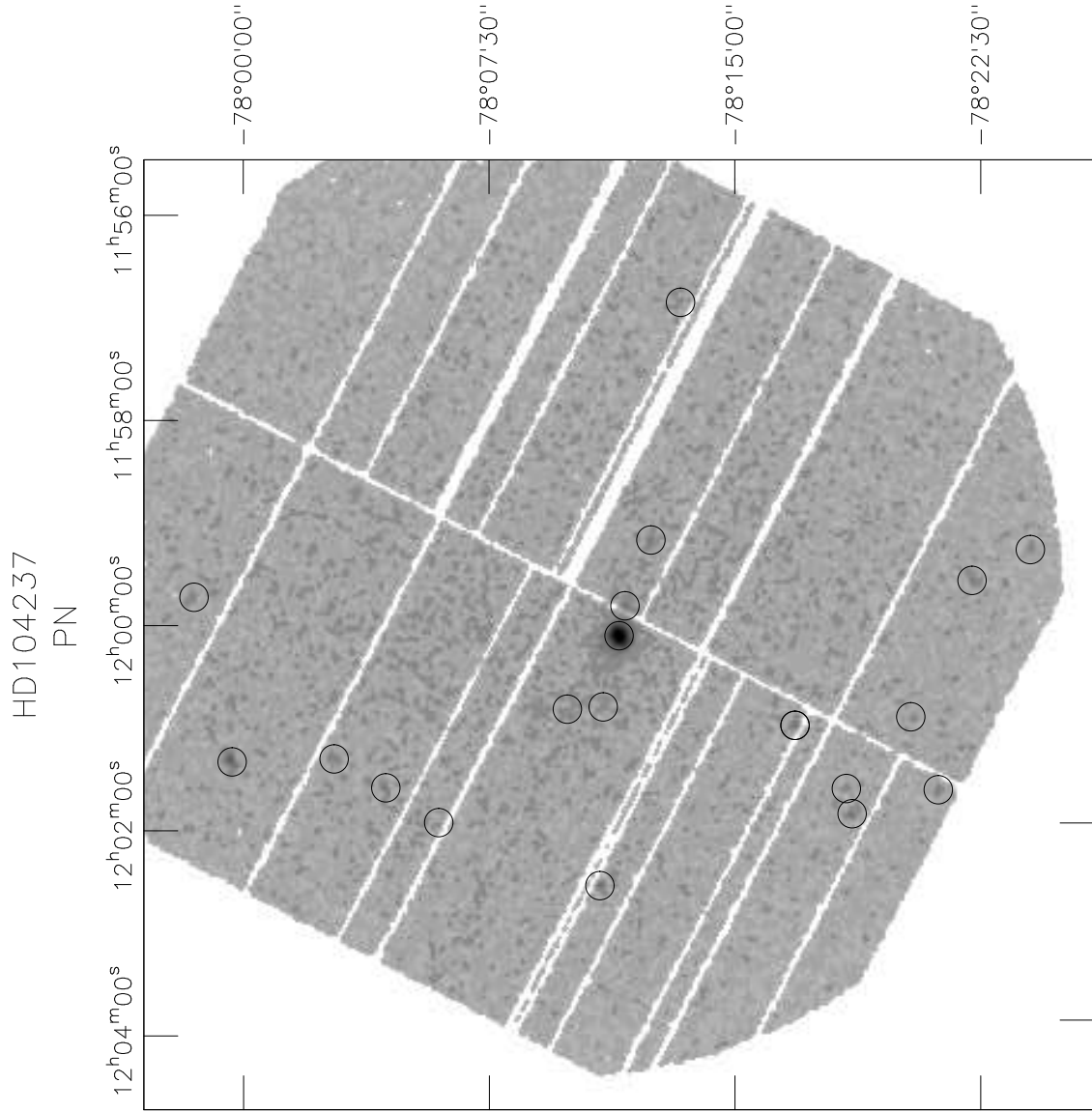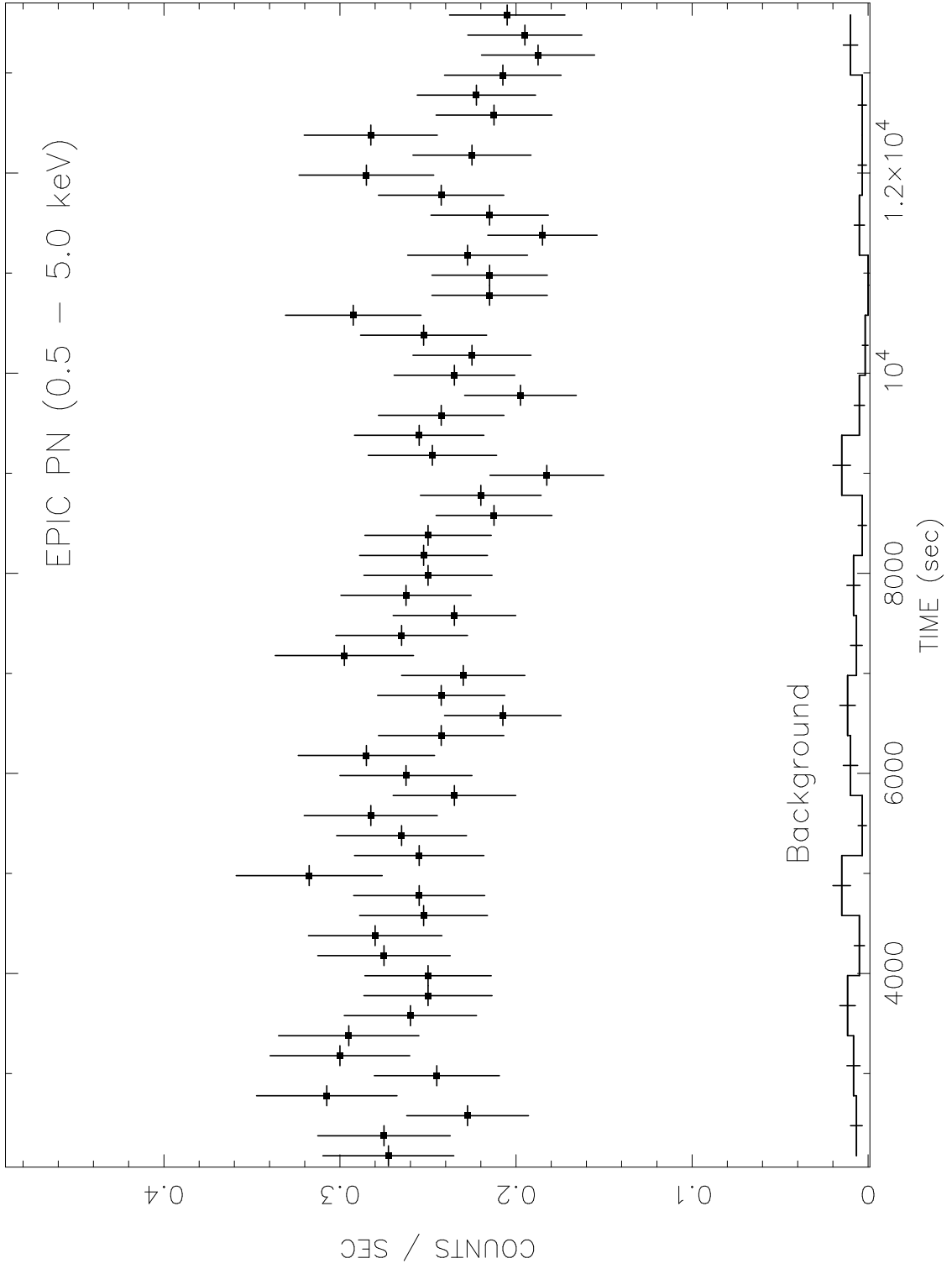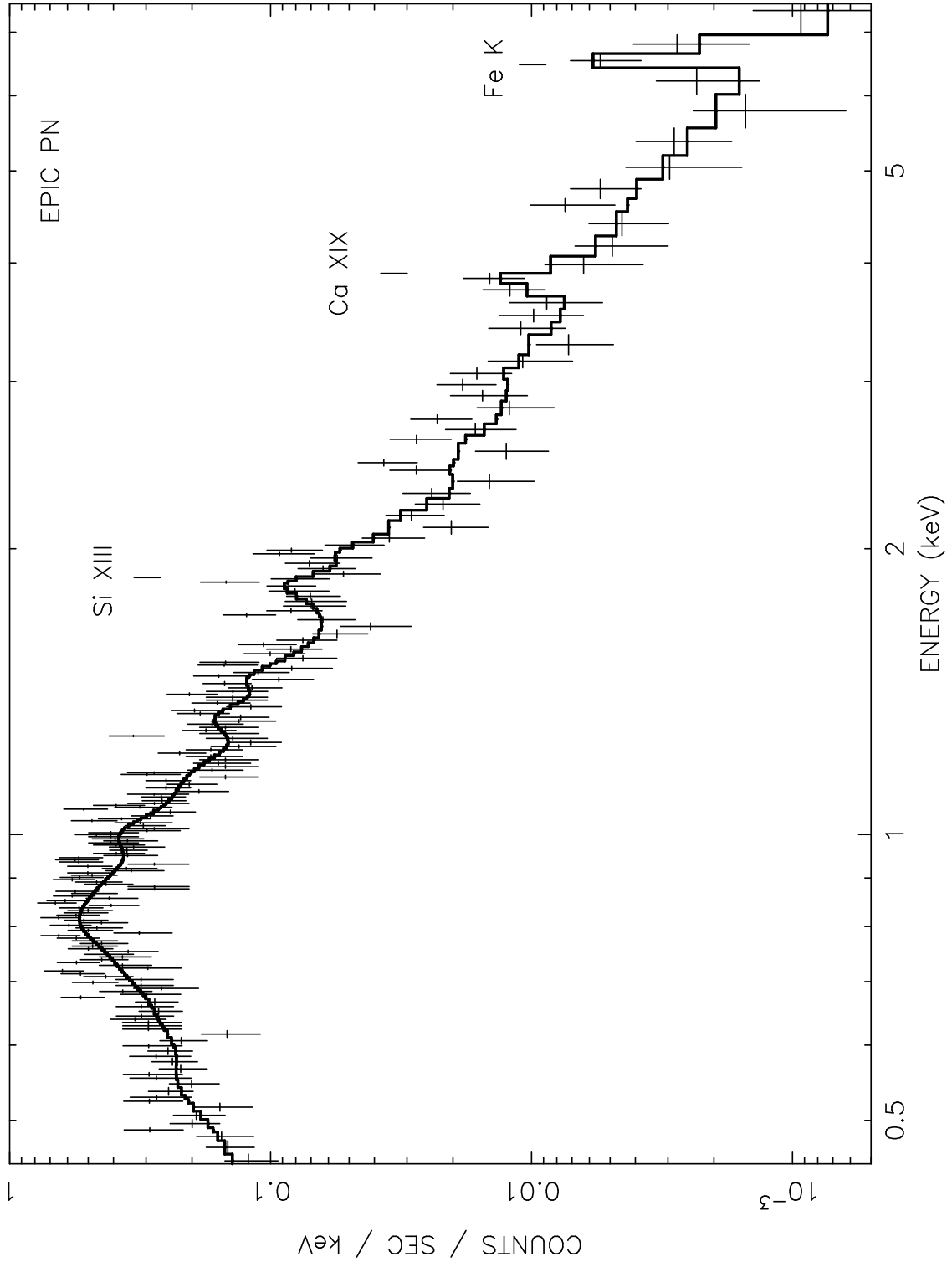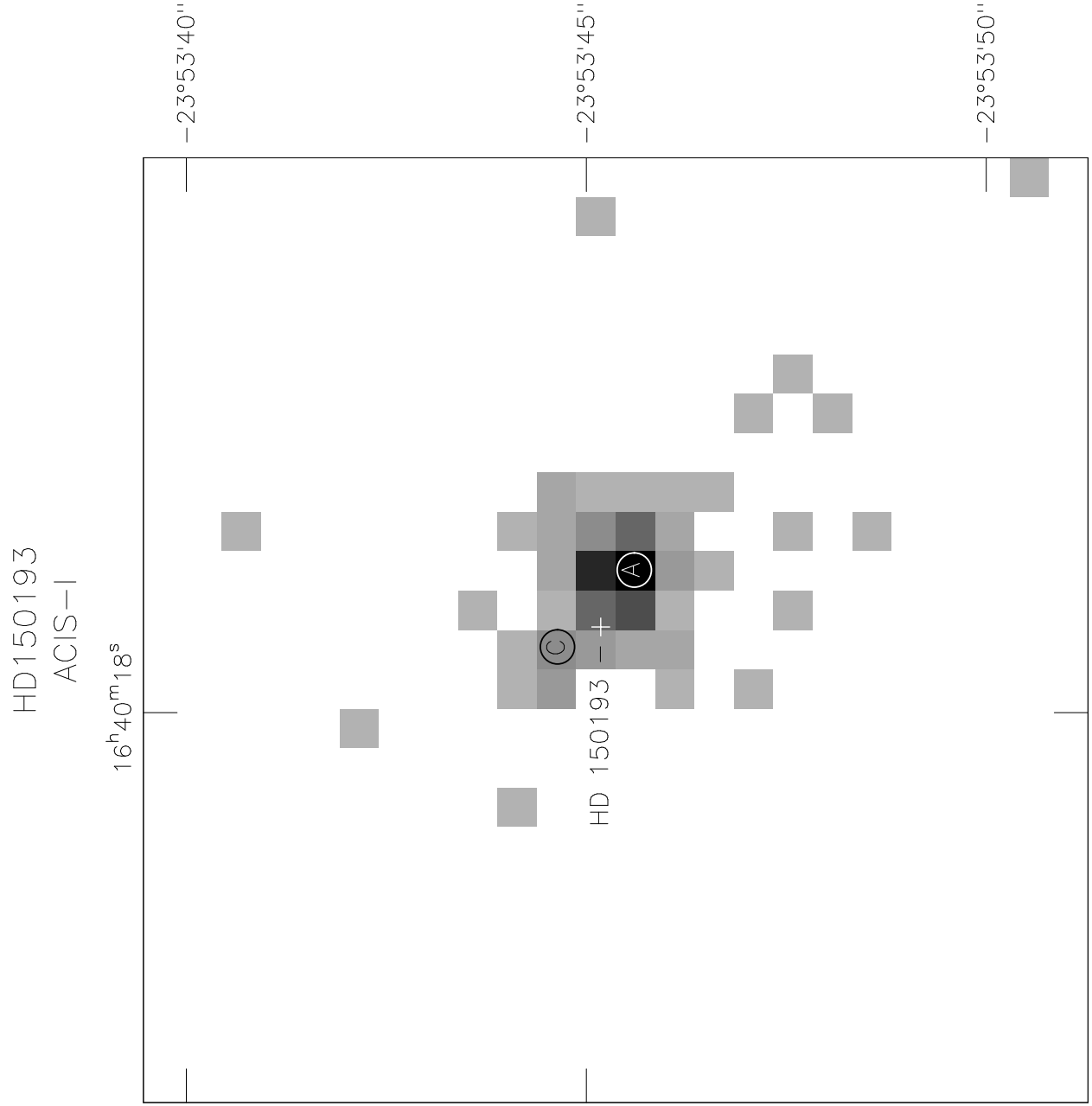
Fig. 1.—

Fig. 2.—

Fig. 3.—

Fig. 4.—

Fig. 5.—

Fig. 6.—

CRA CLOUD CORE
ACIS–I

R CrA

T CrA

Fig. 7.—

Fig. 8.—